Stochastic Simulation of the Suspended Sediment Deposition in the Channel with Vegetation and Its Relevance to Turbulent Kinetic Energy

Liu Yang[1], Wenxin Huai[1], and Yakun Guo[2]

[1] State Key Laboratory of Water Resources and Hydropower Engineering Science, Wuhan University, Wuhan, Hubei 430072, China.

[2] Faculty of Engineering & Informatics, University of Bradford, Bradford, BD7 1DP, UK.

Corresponding author: Wenxin Huai (wxhuai@whu.edu.cn)

Key Points:

- Vegetation-generated turbulent kinetic energy has considerable impact on the sediment deposition probability in vegetated channels.
- Turbulence dominates sediment deposition and resuspension motions when the dimensionless turbulent kinetic energy is larger than its threshold.
- Random displacement model simulates the sediment net deposition in vegetated channel flows with the deposition and resuspension model.

Abstract

The aquatic vegetation patch plays a significant role on sediment net deposition in the vegetated channels. Particularly, the flow is decelerated at the leading edge of a patch that tends to induce vertical updraft, that is, a diverging flow region, in which vegetation greatly affects the pattern of sediment net deposition. This study focuses on the simulation of the sediment net deposition in the whole vegetation patch region through an innovative random displacement model, a Lagrange method, with a probability-based boundary condition instead of the reflection or sorption boundary at the channel bottom. The probability model of deposition and resuspension is proposed according to the flow field characteristics in the different regions of the vegetation patch. The variation of the sediment deposition and resuspension with the turbulent kinetic energy is analyzed to illustrate the effect of the turbulence induced by vegetation, represented by the dimensionless turbulent kinetic energy (ψ), on the sediment deposition and resuspension. The sediment deposition predicted by the proposed model agrees well with the experimental measurements. Results show that the effect of vegetation on the sediment deposition and resuspension motions begins to prevail when the vegetation-induced ψ is larger than its threshold, ψ_*. Although the experimental data are limited, the threshold of ψ is predicted to be within 6.8 to 10 according to the simulation results. As the turbulent kinetic energy increases, the deposition probability decreases continuously when $\psi>\psi_*$.

Keywords

Deposition; Resuspension; Turbulent kinetic energy; Random displacement model; Vegetation patch; Probability model

1 Introduction

The turbulent vortices in the vegetated open channel flow are mainly generated by the vegetation and are remarkably larger than the vortices induced by the bed shear stress in the channel without vegetation (Ghisalberti & Nepf, 2004). Aquatic vegetation also plays an important role in the suspended sediment transport (Huai et al., 2020), bed-load sediment transport (Yang & Nepf, 2018) and sediment deposition and bed form (Yang & Nepf, 2019). Sediment deposition in the vegetated channel flows is receiving considerable attention in recent decades (Mark et al., 1983; Beuselinck et al., 2000; Follett & Nepf, 2018; Kim et al., 2018). There are two opposite effects of the aquatic vegetation on the sedimentation. Aquatic vegetation usually enhances the sediment deposition and produce a region of sediment retention; while they also generate additional drag and obstruction which restrains flow velocity and reduces the sediment carrying capacity (Abt et al., 1994; Gacia et al., 2003; Zong & Nepf, 2010; Zhang et al., 2020). However, some researchers also observed that the reduction of deposition occurred in the vegetation region as many vortices were generated by the vegetation stems comparing with the flow in the bare-bed channel (Follett & Nepf, 2012; Lawson et al., 2012; Ganthy et al., 2015). Improvement of the sediment management in natural rivers, such as sediment retention and erosion in the vegetation region, is important for river management. As such, understanding of the impact of the aquatic vegetation on the sediment deposition and resuspension is essential in order to predict retention or erosion.

Extensive studies have been conducted using various methods to investigate the impact of the aquatic vegetation on the sediment deposition. Among these studies, laboratory experiment is the most popular methodology to investigate the sediment deposition in the vegetated channel flows. Follett and Nepf (2018) conducted experiments to study the retention of the graded sediment particles in a submerged meadow. They found that both the position of particles released and the particle size affected the pattern of sediment retention. Zhang et al. (2020) and Zong and Nepf (2010) also studied the sediment deposition in the channel with vegetation through laboratory flume experiments. Zhang et al. (2020) focused on investigating the effect of the submerged vegetation density and flow velocity on the deposition pattern, while Zong and Nepf (2010) described the effect of the emergent vegetation on the sediment deposition. Though it is convenient and direct to obtain the pattern of the sediment deposition in the vegetation patch using the laboratory flume experiment, its inefficiency and scale effect restrain the development of studies. With the development of the computing resources and the computational fluid dynamics techniques, numerical models have also been widely developed and applied to simulate various turbulent flows. However, to the authors' best knowledge, numerical studies on the sediment deposition in the vegetation patch are still limited (Tsujimoto, 1999; Kim et al., 2018). These two studies developed a depth-averaging two-dimensional (2-D) model to analyze the profile pattern of the sediment deposition in the vegetation region. However, the depth-averaging model is only suitable for shallow water in a relatively wide channel, while many vegetated channel flows are not shallow water flow. As such, the present study attempts to explore the application of the random displacement model to investigate the sediment deposition in the channel with the vegetation patch, not just in the shallow water channels. The random displacement model, which is a Lagrange method, was developed to study the profile of the suspended sediment concentration in the channels with vegetation by the authors (Huai et al., 2019) who expanded the model to study the suspended sediment transport in the vegetated channel flows; and Follett et al (2019) studied the retention of pollen in the flow with different released height of particles through random displacement model. This study will further explore the application of the random displacement model to the sediment deposition pattern in the vegetated sediment laden flows.

Two sediment movement processes, that is, the deposition and the resuspension, are introduced to explore the pattern of the sediment net deposition in the channel with vegetation. Resuspension will occur if the instantaneous velocity near the channel bed is larger than the critical velocity of the sediment incipient motion. Obviously, the net deposition is reduced with the increase of the sediment resuspension. The models involved in the sediment incipient motion are usually based on the bed shear stress τ, such as the most prevalent Shields number θ (Beheshti & Ataie-Ashtiani, 2008; Tinoco & Coco, 2016; Guo, 2020), which is the most representative achievement and is still widely used. However, the stress model has been shown to be inaccurate in terms of the channel with bed forms and vegetation (Nelson et al., 1995; Yager & Schmeeckle, 2013). Some recent studies show that it is the turbulence rather than the bed shear stress which dominates the sediment transport (Houssais et al., 2015) and this situation is more evident in the vegetated channel flows. In the bare-bed channel, the turbulent kinetic energy linearly relates to the bed shear stress (Stapleton and Huntley, 1995), while the turbulent kinetic energy in the vegetated channel flows is primarily generated by the aquatic vegetation (Tanino & Nepf, 2008) and causes τ being no longer a substitute for turbulence. Thus, the turbulent kinetic energy model is widely used to simulate the onset motion of the sediment in the vegetation channel flows in recent decades (Yang et al., 2016; Tinoco & Coco, 2018; Tang et al.,

2019; Yang & Nepf, 2019; Zhang et al., 2020). Yang et al. (2019) predicted the turbulent kinetic energy k in the vegetated channels from a depth-average velocity U and vegetation density, i.e. volume fraction ϕ. Their results demonstrated that the application of the turbulent kinetic energy provided a good prediction of the bed load transport rate. Tinoco and Coco (2018) focused on investigating the relationship between the turbulent kinetic energy and resuspension using the laboratory experiments. They emphasized that the turbulent kinetic energy induced by the flow-vegetation interactions, rather than bed shear stress by mean velocity, was the main driver of the resuspension within the array. Previous studies have only focused on the expression of the turbulent kinetic energy and the relationship between the turbulent kinetic energy and the resuspension or the bed-load transport rate. However, studies about the turbulent kinetic energy and the deposition probability are still rare, which motivates the present study.

This study aims at improving the turbulent kinetic energy model in order to simulate the sediment deposition and the resuspension in the vegetated channel flows through an innovative random displacement model. The main contributions of this study include several aspects. First, this study applies the random displacement model to investigate the sediment deposition, thereby extending the application of the model and providing a new research methodology for the sediment deposition. Second, we propose a deposition and resuspension probability model based on the previous turbulent kinetic energy models. The probability of the sediment deposition and resuspension varies from the leading edge of the vegetation patch to the end of the patch according to the flow field features in the different vegetation patch regions. Third, the results of the present study demonstrate the dominant effect of the aquatic vegetation on the sediment deposition when the value of the dimensionless turbulent kinetic energy is larger than the proposed threshold ψ_*. The model is validated with the net deposition measured in the laboratory flume, showing the accuracy of the proposed model in predicting the sediment net deposition in the vegetated channels.

2 Method

2.1 Numerical Model

In this study, a random displacement model is applied to trace the particles in the open channel flows with the aquatic vegetation. Recently, Huai et al. (2019) developed the random displacement model to simulate the suspended sediment concentration in the vegetated channel flows. This study tracks the motion of sediment particles in the vegetated channels with the sediment deposition being innovatively considered at the bottom of the channel. Though details of the random displacement model can be found in Huai et al. (2019), we provide a brief conception of the random displacement model for convenience and completeness.

For the vertical 2-D simulation, the displacement of the sediment particles is modeled as follows:

$$\Delta x = u(z)\cdot\Delta t\,, \tag{1}$$

$$\Delta z = (\frac{dK_z(z)}{dz} - \omega)\cdot\Delta t + w\Delta t + R\sqrt{2K_z(z)\Delta t}\,, \tag{2}$$

where x and z [L] are the longitudinal and the vertical coordinates, respectively; Δx and Δz [L] are the displacements of the sediment particles in the longitudinal and the vertical directions,

143 respectively; Δt [T] is the time step; K_z [L^2T^{-1}] is the turbulent diffusion coefficient that expresses
144 the strength of the turbulent vortex; w and u [LT^{-1}] is the vertical and longitudinal flow velocity,
145 respectively; R [-] is a normally distributed random number with mean 0 and standard derivation
146 1; and ω [LT^{-1}] is the settling velocity of the sediment particles, which is estimated from
147 equation (4) in Cheng (1997).

148 The random displacement model is a Lagrangian method, and the option of the boundary
149 condition is significant for the accuracy of the model. The water surface is set as the reflection
150 boundary (Liu et al., 2018; Huai et al., 2019). However, to accurately simulate the sediment
151 deposition, the reflection boundary is unsuitable for the bottom bed of the channel. This is
152 considerably different from settings in previous studies.

153 In the present vertical 2-D model, the advection-diffusion equation of the sediment is:

$$\frac{\partial C}{\partial t}+\frac{\partial (uC)}{\partial x}+\frac{\partial (wC)}{\partial z}-\frac{\partial}{\partial x}\left(K_x\frac{\partial C}{\partial x}\right)-\frac{\partial}{\partial z}\left(K_z\frac{\partial C}{\partial z}\right)-\frac{\partial(\omega C)}{\partial z}+S=0, \tag{3}$$

154 where t [T] is the time; K_x is the longitudinal dispersion coefficient; C [ML^{-2}] is the time-spatial
155 averaging suspended sediment concentration and S [$ML^{-2}T^{-1}$] represents the source term. In
156 Equation (3), the longitudinal dispersion term could be ignored because the magnitudes of the
157 term is considerably smaller than the longitudinal advection term. The sixth term in the left hand
158 side of Equation (3) represents the settling term, which highlights the difference between the
159 sediment particles and pollutants (whose settling velocity is usually ignored).

160 The initial and boundary conditions are as follows:

$$C(0,x,z)=C_0\phi_0(z)\delta(x), \tag{4}$$

$$K_z\frac{\partial C(t,x,0)}{\partial z}=-\eta C(t,x,0), \tag{5}$$

$$\frac{dC(t,x,H)}{dz}=0, \tag{6}$$

161 where C_0 is the initial sediment concentration; $\phi_0(z)$ is the initial distribution function of the
162 sediment particles in the vertical direction (uniform distribution is used in this model); $\delta(x)$ is the
163 Dirac delta function, which means that all sediment particles are released at x=0; H [L] is the
164 flow depth; and η [LT^{-1}] is the sediment deposition rate at the bottom of the channel. Equation
165 (5) considers the deposition boundary condition at the channel bed by introducing the parameter
166 η, which expresses the comprehensive influence, including settling velocity and flow field, on
167 the sediment deposition. In terms of Equation (6), the reflection boundary condition is specified
168 at the water surface.

169 The bottom boundary condition can be rewritten as:

$$\frac{\partial C(t,x,0)}{\partial z}=-\frac{\eta}{K_z}C(t,x,0). \tag{7}$$

170 In order to understand the conception of the boundary condition at the channel bottom, the
171 deposition boundary can be removed if the sediment concentration near the river bed satisfies the
172 following:

$$\frac{C(t,x,dz/2)-C(t,x,-dz/2)}{C(t,x,dz/2)} \approx \frac{dC(t,x,0)}{C(t,x,0)} = -\frac{\eta}{K_z}dz \quad . \tag{8}$$

Equation (8) is the finite-differential form of the concentration gradient at z=0 when dz approaches to zero. The conception diagram for the deposition probability is shown in Figure 1 with a virtual deposition layer. The real channel bottom can be replaced by a virtual deposition boundary by adjusting the sediment concentration to meet the requirement of Equation (8). From this assumption, the sediment particles can pass through the virtual boundary and enter into the virtual deposition layer, where the sediment particles are supposed to be deposited, i.e. the bed load.

As the value of dz in the Equation (8) is negative, the deposition probability of a particle at the bottom of the channel can be expressed as:

$$P_d = \frac{C(t,x,dz/2)-C(t,x,-dz/2)}{C(t,x,dz/2)} = \left|\frac{-\eta}{K_z}dz\right| , \tag{9}$$

where P_d [-] is the deposition probability of the sediment particles expressing the comprehensive effects of vegetation on flow field and can be obtained from the numerical simulation.

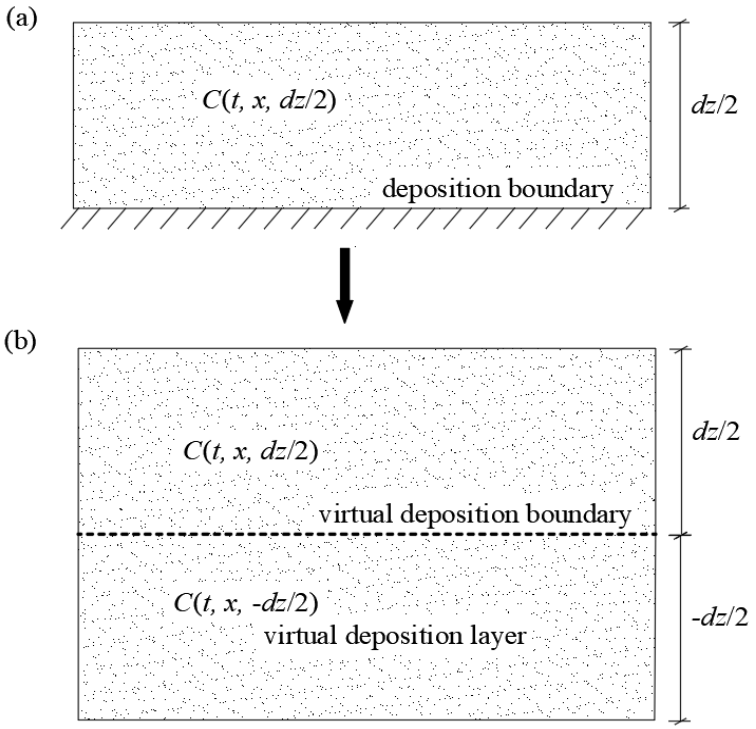

Figure 1 Conception of the sediment particle deposition probability. In Figure 1(a), the sediment particles cannot pass through the boundary and deposit at the boundary according to the deposition probability. In Figure 1 (b), the particles can go through the virtual deposition boundary by controlling the sediment concentration consistent with Equation (8), where the same effects with Figure 1(a) can be obtained.

2.2 Flow Field Domain

Aquatic vegetation patch, acting as a barrier, considerably alters the flow field structure, as shown in Figure 2. In submerged vegetated channel flows, the flow velocity is decelerated when water flow enters into the submerged vegetation patch. Meanwhile, the flow deceleration triggers a vertical updraft where the vertical velocity w sharply increases. This flow adjustment begins at the entrance edge of the vegetation patch and develops along the permeating the vegetation region. This flow adjustment then completes at the position $x=x_D$, where the updraft approximates to vanish. According to the study of Chen et al. (2013), the adjustment length x_D [L] is a function of the vegetation density, the flow depth and the drag coefficient:

$$x_D = (6.9 \pm 1.1)(1-\phi)h + \frac{3.0 \pm 0.4}{C_D a}(1-\phi) \quad , \tag{10}$$

where ϕ [-] is the solid volume fraction within the vegetation region, a [L^{-1}] is the front area of vegetation per volume, h [L] is the height of vegetation and C_D [-] is the drag coefficient induced by vegetation.

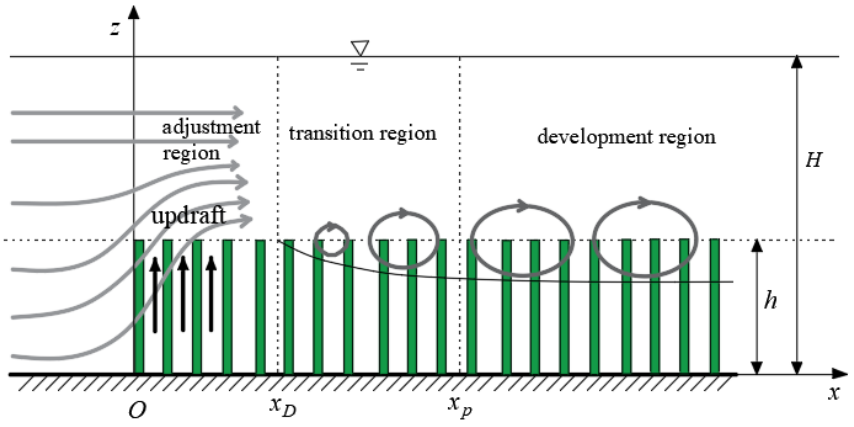

Figure 2 Sketch of the flow field structure in the vegetation patch. The flow field is divided into three regions according to the flow features: adjustment, transition, and development regions.

Velocity decreases suddenly near the top of the vegetation due to the barrier effect induced by the vegetation on the velocity within the patch region. At the same time, overflow is accelerated. Therefore, a shear layer with coherent vortex structure begins to develop within the adjustment region. The development of the shear vortex is constrained within the adjustment region by the vertical updraft (Raupach et al., 1996; Ghisalberti, 2002). For this reason, the shear vortex, i.e. the mixing layer, begins to develop at the end of the adjustment region x_D and reaches the highest scale of vortex at $x=x_p$, as shown in Figure 2. Downstream the position x_p, the flow structure reaches a developed state. The length of x_p depends on the scale of the vortex structure and is determined by the vegetation density and the depth of submergence (Chen et al., 2013). Details on determining the value of x_p can be found in Chen et al. (2013).

The discussion above demonstrates the complexity of flow field structure in the channel with vegetation. According to the governing equation of the random displacement model, i.e. Equations (1 and 2), the flow field parameters, namely the flow velocity and turbulent diffusion coefficient, are vital for the particles motion. In order to obtain the complex flow field

parameters, in present study, realizable k-ε turbulence model and porous model are used to simulate the flow field in vegetated channels. The vegetation region is simulated as a porous zone by adding drag force terms to the momentum equations. The drag force term exerted by vegetation can be modeled as:

$$f_i = \frac{1}{2}\frac{C_D a}{1-\phi}\overline{u}_i\sqrt{\overline{u}_j\overline{u}_j}\,. \tag{11}$$

Where f_i is the vegetation induced drag in the x_i direction; $\overline{u}_i$ is the temporal averaged velocity component in the x_i direction. More information about the porous model and coefficient C_D can be found in Ai et al (2020).

As for the turbulent diffusion coefficient, it is very complicated in the channel with submerged vegetation. In the present study, to simplify the model, the turbulent diffusion coefficient is approximated as the same as the profile of Huai et al (2019) in the transition and developed regions. They determined turbulent diffusion coefficient in several typical position, i.e. top of vegetation (Ghisalberti & Nepf, 2005) and wake region in the vegetation zone (Nepf et al., 2007), according to the previous experimental research outcomes; and then linearly connected several positions. This turbulent diffusion coefficient model has been used and verified by many researchers (Follett & Nepf, 2016; Huai et al., 2019). In the adjustment region, the vertical flow velocity dominates the vertical mass transport as the effect of updraft is larger than diffusion. In present model, it is reasonable to ignore the vertical turbulent diffusion term in this region, which could also be verified from the agreement between simulated sediment deposition and experiment measurements deposition.

It is important to note that the flow velocity u and w in submerged vegetated channel flows are simulated with above porous and turbulence models; however, flow velocity and turbulence diffusivity in the channel with emergent vegetation are not simulated with the model. Previous researchers showed that the longitudinal velocity (Huai et al., 2009) and turbulent diffusion coefficient (Nepf, 2012) are nearly a constant in the channel with emergent vegetation; and the vertical velocity is around zero even though in the leading region of vegetation. Therefore, in present study the measured value is approximately used in whole flow field domain in the channel with emergent vegetation.

2.3 Deposition and Resuspension Probabilities

Gacia et al. (2003) and Zhang et al. (2020) showed that the vegetation sometimes enhances the sediment deposition in channel with submerged meadows. However, some studies illustrated that the vegetation contributed to erosion and weakened the deposition in the leading of circular emergent patch comparing with the bare bed flows (Follett & Nepf, 2012). The profile of sediment particles in the channel bed is closely associated with the amount of the deposition and resuspension. In the present study, the effect of flow field on the deposition and the resuspension is represented by the probability of the deposition and resuspension in different regions of vegetation. The probability model of the sediment deposition and the resuspension is proposed in the present study according to the flow field structure in the vegetation patch.

2.3.1 Deposition Probability

The deposition of the sediment particles is affected by the flow field in the vegetated channel flows. The characteristics of the flow field vary considerably at different regions of vegetation. Because the effect of updraft on the deposition decreases along the distance to the patch entrance, we assume that the deposition probability increases gradually from zero at the leading edge of vegetation; and the deposition probability is assumed as a constant beyond the adjustment region because the updraft disappears gradually with the shear vortex development. Three different expressions of the deposition in the adjustment region, i.e. $x<x_D$, are then assumed as follows:

$$P_d = -\frac{P_{d1}}{x_D^{\,2}} x^2 + \frac{2P_{d1}}{x_D} x, \tag{12}$$

$$P_d = \frac{P_{d1}}{x_D^{\,2}} x^2, \tag{13}$$

$$P_d = \frac{P_{d1}}{x_D} x, \tag{14}$$

where P_{d1} [-] is the deposition probability outside the adjustment region. Figure 3 illustrates these hypothetic probability profiles. In this model, P_{d1} is the only unknown parameter, which will be determined according to the consistency between the simulated and measured net deposition. The best suitable expression of the deposition probability in the adjustment region will be validated in the later section through comparing observed sediment net deposition and simulated net deposition with Equations 12, 13 and 14.

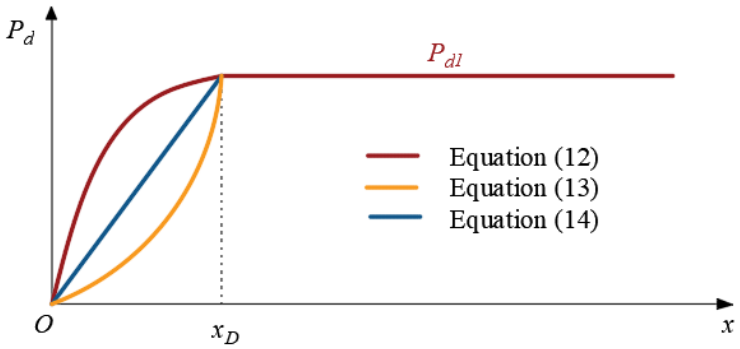

Figure 3 Diagram of three hypothetic profiles of sediment deposition probability.

2.3.2 Resuspension Probability

Yang et al. (2016) derived the critical velocity of the incipient sediment motion from the turbulent kinetic energy. In the bare bed flow, the incipient sediment motion mostly depends on the bed shear stress; therefore, the critical velocity is historically related to the bed shear stress (Recking, 2009; Houssais et al., 2015), e.g. critical Shields number θ_c [-]. The studies of Stapleton and Huntley (1995) showed that the role of turbulence is inherently represented in the Shields diagram because the turbulent kinetic energy and the shear stress are linearly related in a bare-bed channel. In the vegetated channel flows, however, vegetation stems predominate the

283 production of the turbulence (Tanino & Nepf, 2008); thus the shear stress is no longer alternative
284 by the near-bed turbulence, i.e. the turbulent kinetic energy. Recently, many studies have
285 attempted to prove the effects of turbulence on the incipient sediment motion (Diplas et al.,
286 2008; Yang et al., 2016; Tang et al., 2019). For example, according to the study of Yang et al.
287 (2016) conducted in current, the depth-averaging critical velocity in the vegetated channels was
288 estimated as follows:

$$U_c = \frac{U_{c0}}{\sqrt{1+\frac{\delta^2}{C_b}\left(\frac{2C_D\phi}{\pi(1-\phi)}\right)^{2/3}}}, \tag{15}$$

289 where U_{c0} [LT^{-1}] and U_c [LT^{-1}] denote the depth-averaging critical velocity in the bare bed flow
290 and the vegetated flow, respectively; coefficient C_b=C_f/2 [-] (C_f is the bed friction coefficient);
291 and δ [-] is a scale factor.

292 The sediment resuspension probability is derived from the critical velocity of the
293 incipient sediment motion and the probability density function of the instantaneous flow
294 velocity. As shown in Equation (15), the depth-averaging velocity is most commonly used as the
295 criterion for the sediment incipient motion. Dou (1960) derived the following formula of the
296 sediment incipient motion based on the balance of forces acting on the sediment particle:

$$U_c = 0.408\left(\ln(\frac{H}{k_s})\right)\left((s-1)gd_{50}+0.19\frac{\varepsilon_k+gH\delta_p}{d_{50}}\right)^{1/2}, \tag{16}$$

297 where g [LT^{-2}] is the acceleration of gravity; d_{50} [L] is the median size of the sediment particles;
298 k_c=1.437 is a constant parameter; s [-] is the ratio of the bulk sediment density over water
299 density; δ_p=0.213×10^{-6} [L] is the thickness of pellicular water; k_s [L] is the roughness height of
300 bed (k_s=0.0005 m if d_{50}<0.5 mm); and ε_k [L^3T^{-2}] (usually 2.56 × 10^{-6} m^3s^{-2}) is a comprehensive
301 parameter of cohesive force.

302 Previous studies showed that the depth-averaged velocity was a valid criterion for
303 majority of sediments onset motion. However, the present model pays more attention to every
304 single particles motion, especially in the region near the riverbed. Therefore, it is precise to take
305 the near-bed velocity as the criterion of sediment onset motion rather than depth-averaged
306 velocity. The different turbulent intensity leads to a variation of the probability density function
307 of the flow velocity at the vegetation and overflow regions (Nezu & Nakagawa, 1993). As such,
308 the velocity near the bottom of the channel, u_b, instead of the depth-averaging flow velocity, is
309 used as the criterion to determine whether the sediment resuspension occurs or not (Marion &
310 Tregnaghi, 2013). The sediment at the position of two times sediment particle size above the
311 riverbed is regarded as the suspended sediment; therefore, the flow velocity at z=2d_{50} is assumed
312 as the near-bed flow velocity u_b. The critical depth-averaging flow velocity, Equation (16), is
313 then transformed to the critical near-bed velocity, u_{b_c}, according to the rate of the depth-
314 averaging velocity and the near-bed velocity on the exponential velocity profile:

$$u_{b\_c} = 0.476(2d_{50})^{1/6}H^{-7/6}\left(\ln(\frac{H}{k_s})\right)\left((s-1)gd_{50}+0.19\frac{\varepsilon_k+gH\delta}{d_{50}}\right)^{1/2}. \tag{17}$$

315 The critical near-bed velocity, u_{b_c}, calculated by Equation (17) will be used to determine
316 the inception of the sediment resuspension. To clarify the relationship between the turbulent
317 kinetic energy induced by the vegetation and the sediment resuspension, we analyze the
318 simulated results and the variation of the turbulent kinetic energy that actually affects the
319 variation of the flow velocity.

320 The incipient motion criterion, i.e. the critical velocity, is transformed into the
321 resuspension probability of the sediment particles according to the fluctuation of instantaneous
322 velocity. Assuming that the instantaneous near-bed flow velocity u_b is approximate to the normal
323 distribution (Choi & Kwak, 2001), the probability density function of u_b can be derived as
324 follows:

$$f(u_b) = \frac{1}{\sqrt{2\pi}\sigma} e^{-\frac{1}{2}\frac{(u_b-\overline{u_b})^2}{\sigma^2}}, \tag{18}$$

325 where $\overline{u_b}$ [LT^{-1}] is the time-averaging near-bed flow velocity and $\sigma = \sqrt{(u_b - \overline{u_b})^2}$ is the standard
326 deviation in which σ=1 is usually used. When the instantaneous velocity is larger than the critical
327 velocity of the incipient motion, the resuspension of the sediment particles takes place as shown
328 in Figure 4. The resuspension probability P_s, therefore, can be simulated as follows:

$$P_s = 1 - P(u_b < u_{b\_c}) = 1 - \int_{-\infty}^{u_{b\_c}} \frac{1}{\sqrt{2\pi}\sigma} e^{-\frac{(u_b-\overline{u_b})^2}{2\sigma^2}} du_b . \tag{19}$$

329 In the present model, sediment particles reaching river bed firstly deposit according to the
330 deposition probability model, and then some are re-suspended according to the resuspension
331 probability model. From the model and resuspension concept, the deposition motion is the
332 foundation of resuspension motion. We assume that the resuspension probability is a constant
333 calculated by Equation (19) in the whole domain and therefore, we emphasize the effect of
334 deposition probability to study the main factors that impact the net deposition, i.e. deposition
335 probability.

336

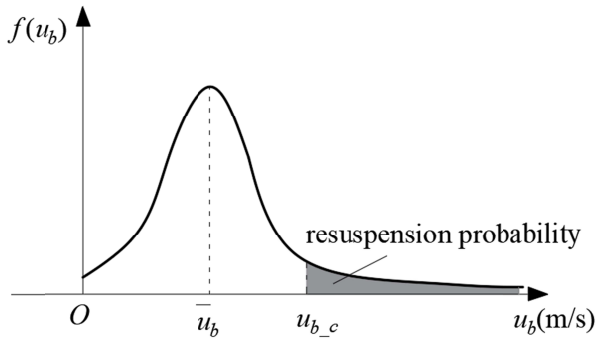

337
338 **Figure 4** Probability density function of u_b and the diagram of the resuspension probability.

339

3 Results

The numerical modelling procedure mainly includes three steps: (I) the flow field is modeled with the realizable k-ε model and porous model; (II) the random displacement model is performed using governing equations of sediment particles motion, i.e. Equations (1) and (2), associating with calculated flow field data in the first step and the simplified turbulent diffusion coefficient; (III) the value of unknown deposition probability P_{d1} is fitted through the comparison of simulated deposition and experimental deposition. The proposed model is then applied to simulate the deposition of the sediment particles in the vegetated channel flows and is validated by comparing the simulated results with the measurements in several available laboratory experiments, which are briefly described below.

3.1 Validations

3.1.1 Flow Field

The experiments conducted by Zhang et al. (2020) are used to verify the flow field model. Zhang et al. (2020) conducted experiments to study the sediment deposition profiles in the submerged long meadows for different flow and vegetation density conditions. The numerical domain is chosen as a 0.36 m high and 10 m long two-dimension region, and the vegetation zone is 0.07 m high and 8.4m long. In the model, the finest mesh size is 5 mm$\times$5 mm in the vegetation zone. Taking the case 3 as an example, experimental parameters are listed in Table 1, where U [LT^{-1}] is the depth-averaging flow velocity and U_1 represents the mean longitudinal velocity within vegetation region.

Table 1 Experimental parameters of case 3 in experiments of Zhang et al. (2020).

Condition	H (m)	h (m)	U (m/s)	U_1 (m/s)	ϕ(-)	C_D (-)	x_D (m)	x_p (m)
Case 3	0.36	0.07	0.16	0.04	0.048	1.3	0.80	4.65

Figure 5 shows the good agreement between the simulated and measured longitudinal velocity u at position x=5 m. In the vegetation region, the simulated longitudinal velocity is slightly larger than experimental data. Although the porous model could simulate the effect of vegetation by extra drag force, the absence of real structure of vegetation weakens the impact of vegetation, which is likely to account for the overestimation of the modeled velocity in the vegetation zone. This means that the decrease of velocity with the impact of the vegetation obstacle in the present model is weaker than experiments. Nevertheless, the calculated velocity could accurately reproduce the main flow characteristics in channels with submerged meadows.

Figure 6 demonstrates the modeled u and w, where the dash lines express the vegetation zone. u decreases within the region of vegetation, while the velocity of overflow is accelerated (Figure 6(a)). The vertical diversion could be founded in head of vegetation patch according to Figure 6(b). According to the agreement of results, the porous and realizable k-ε models are validated to perform well on the simulation of the flow field in the channel with submerged vegetation.

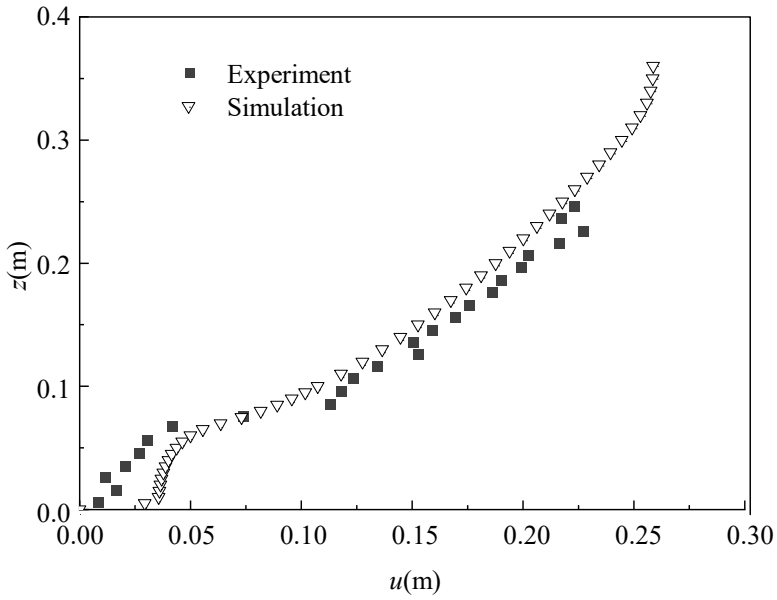

Figure 5 Comparison of simulated and experimental longitudinal velocity at position x=5m.

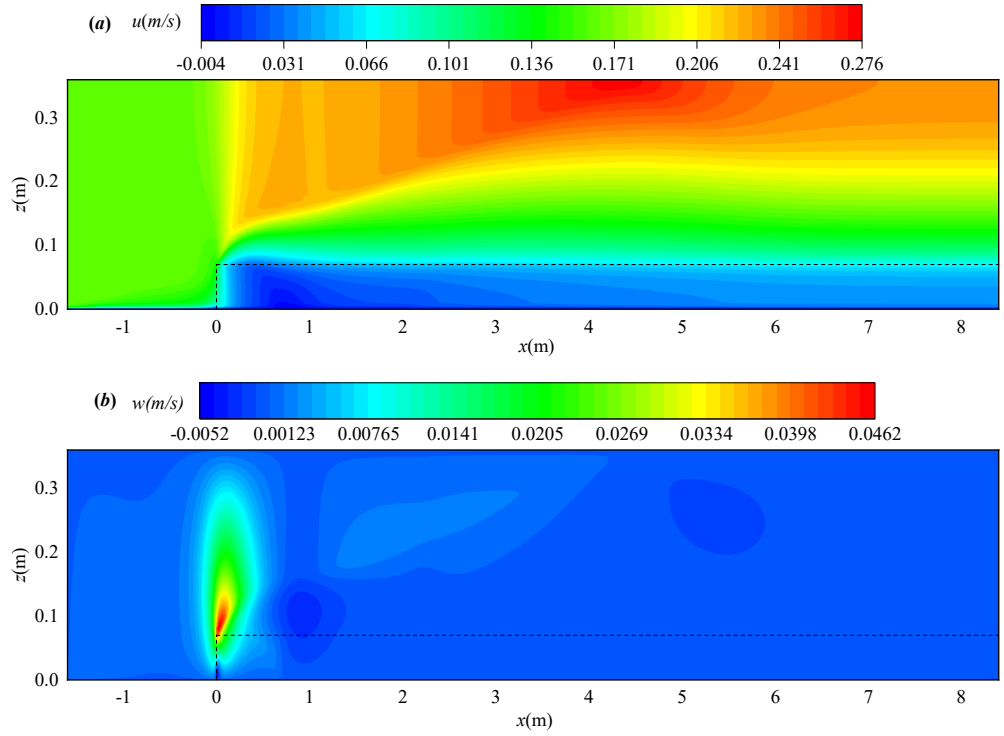

Figure 6 Contour plot of longitudinal and vertical velocity.

3.1.2 Deposition Probability Model

Sediment transport (deposition and resuspension) is calculated using the random displacement model associating with calculated flow field and simplified turbulent diffusion coefficient. The value of unknown deposition probability P_{d1} is fitted through the comparison of

the simulated and measured deposition. In the simulation, 500,000 particles are modeled with the time step of 0.05 s. In random displacement model, the condition at the outlet is assigned as the inlet condition at the next time-step in the computational domain to simulate the sediment transport in the cyclic flume. This means that the sediment particles that pass through the outlet will return back into the inlet and transport in the flume again. The present study models the sediment net deposition in the channel with both the submerged and the emergent vegetation, respectively.

To determine which deposition probability (Equations (12) to (14)) provides good prediction, the simulated sediment net deposition is compared with the experimental measurements. Figure 7 shows the results of the simulated net deposition with three probability profiles (Equations (12) – (14)), taking case 4 (see Table 3 in section 3.2) as example. The mean-root errors, calculated as $MRE = \frac{1}{N}\Sigma\left(\frac{|Dep_e - Dep_m|}{Dep_e}\right)\times 100\%$ (where Dep_e and Dep_{m} [ML^{-2}] are experimental and modeled net deposition respectively and N [-] is the observation number of deposition) are also plotted in Figure 7. It is shown that the MRE with Equation (12) is the smallest within the three profiles, which indicates that the sediment net deposition simulated with Equation (12) is more accurate. Therefore, the deposition probability is expressed as

$$P_d = \begin{cases} -\frac{P_{d1}}{x_D^{\,2}}x^2 + \frac{2P_{d1}}{x_D}x, & x \le x_D \text{ (20-a)} \\ P_{d1}, & x > x_D \text{ (20-b).} \end{cases}$$

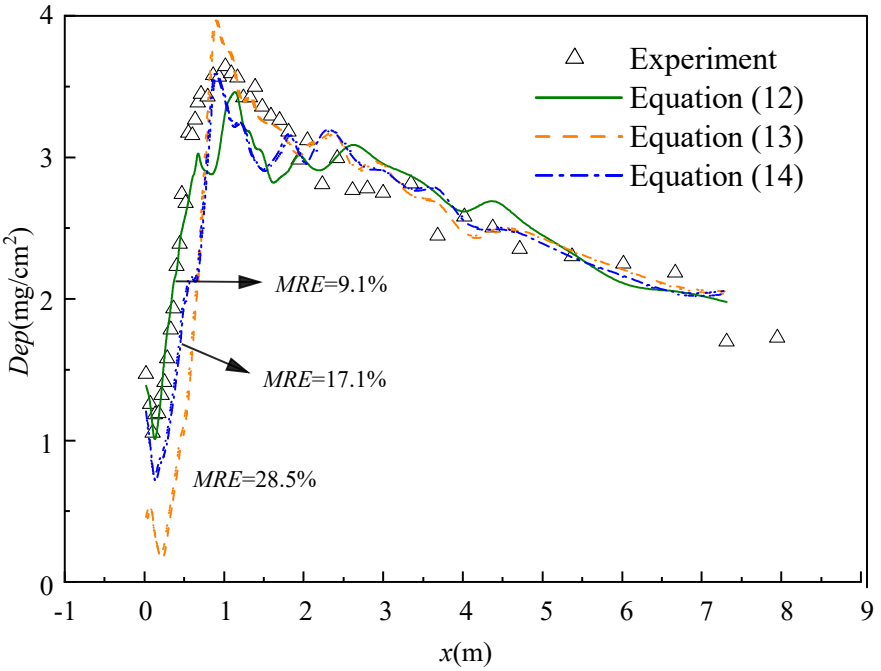

Figure 7 Comparison of the experimentally measured net deposition in Zhang et al. (2020) and simulated deposition with three assumed deposition probability profiles.

3.2 Sediment Deposition

Zong and Nepf (2010) conducted experiments to study the effect of the dense and sparse emergent vegetation on the sediment deposition with vegetation covering half-wide channel. Their experimental parameters are listed in the Table 2, where M_{tot} [M] is the total deposition in the vegetation region. However, the present study does not focus on the lateral profile of the sediment deposition. Instead, we mainly study the deposition patterns along the streamwise direction. The deposition in the center line of vegetation region is approximately thought as the deposition in channel with vegetation, as the main effect region of lateral diversion, i.e. outer region, excludes the center line of vegetation, see Figure (5) in Zong and Nepf (2010). Figure 8 shows the comparison of the simulated and experimentally measured sediment deposition, where *Dep* [ML^{-2}] represents the deposition per unit area. It is seen from Figure 8 that the sediment deposition profile predicted by the proposed model generally agrees with the experimental measurements, which validates the reliability and accuracy of the present model. This also means that the proposed deposition and resuspension probability in this study can correctly reflect the effect of the flow field on the sediment net deposition in the channel with the aquatic vegetation.

Table 2 Experimental parameters in the study of Zong and Nepf (2010)

Conditions	H (m)	U (m/s)	ϕ (-)	x_D (m)	x_p (m)	M_{tot} (g)	P_{d1}(‰)
Z-Dense	0.14	0.005	0.1	2	7.5	86	1
Z-Sparse	0.14	0.014	0.02	3	7.5	95	1

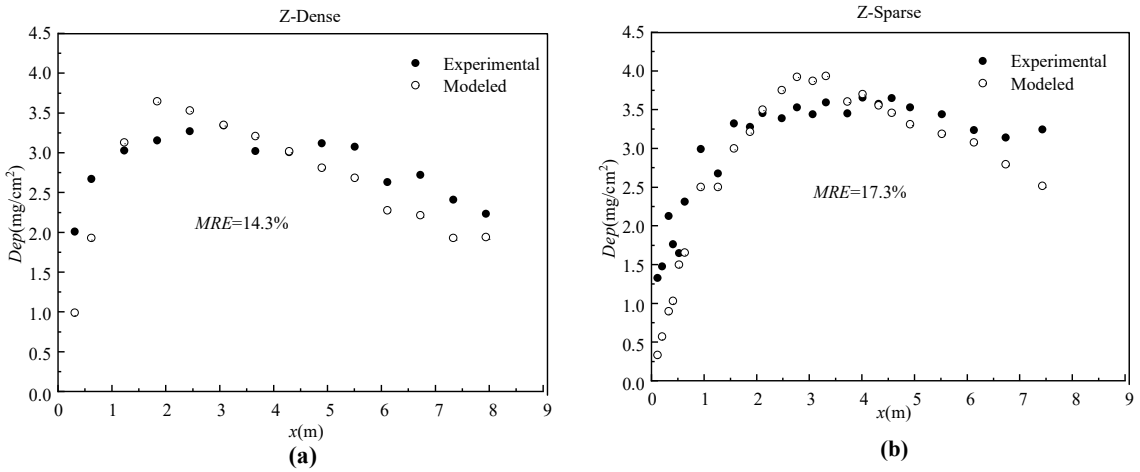

Figure 8 Comparison between the experimentally measured and modeled sediment deposition profiles within the vegetation patch region in the open channel flows. (a) Dense vegetation patch and (b) sparse vegetation patch.

Figure 9 shows the comparison of the simulated sediment deposition profile with the laboratory experiments conducted by Zhang et al. (2020) (see Table 3 experimental parameters in each case) in the meadow along the longitudinal direction. They focused on investigating the effect of the flow velocity and the vegetation density on the sediment net deposition in the vegetation region. For the sake of convenience, the related conditions, such as the vegetation density and the depth-averaging velocity, are also shown in Figure 9.

The results in Figure 9 show that the sediment net deposition is small in the leading edge of the meadow due to the effect of updraft. This net sediment deposition then increases sharply with the increase of the longitudinal distance within a small leading edge region. For cases 1 and 2, the sediment resuspension probability is slightly different from other conditions. Table 1

shows that the velocity for these two cases is much smaller than those of others; therefore, the turbulence intensity is also small. As a result, the effect of the vegetation on the resuspension is trivial. This leads to a zero resuspension probability, which is also confirmed by Zhang et al (2020). Figure 9 also shows that the simulated net deposition is smaller than experimental measurements in the upstream of vegetation. According to the analysis of Zhang et al (2020), for cases 1 and 2, with the lowest velocity, net deposition profiles in vegetation region is the same as the deposition outside vegetation, i.e. spatially uniform pattern. This implies that the effect of vegetation updraft on the deposition patterns is trivial in these conditions. However, the deposition probability model proposed in this study considers the impact of updraft through the gradually increased deposition probability for all conditions, which may account for the deposition differences between model and experiment in the leading of vegetation.

Table 3 Experimental parameters of Zhang et al. (2020)

Conditions	H (m)	h (m)	U (m/s)	U_1 (m/s)	ϕ(-)	C_D (-)	x_D (m)	x_p (m)	M_{tot} (g)	P_{dl} (‰)
Case 1	0.36	0.07	0.06	0.02	0.018	1.4	1.33	4.65	106	2
Case 2	0.36	0.07	0.06	0.03	0.0084	1.3	2.30	3.32	96	2
Case 3	0.36	0.07	0.16	0.04	0.048	1.3	0.80	4.65	101	5
Case 4	0.36	0.07	0.16	0.07	0.018	1.2	1.30	4.65	79	40
Case 5	0.36	0.07	0.16	0.09	0.0084	1.1	2.30	4.65	61	50
Case 6	0.26	0.07	0.22	0.13	0.0084	1.1	2.30	3.32	25	20

Overall, the simulated net deposition is consistent with the measured deposition, especially in the region $x>x_D$. The deviation is more likely to be found in the updraft region, where the vertical flow velocity is stronger than it in the developed region. Although the complex flow structure in the adjustment region complicates the modeling, the net deposition is still well simulated by the proposed model. Furthermore, the simulated results illustrate that both the magnitude and position of the predicted maximum sediment deposition are reasonably consistent with the experimental measurements, although some deviation exists in the simulated and experimental positions where the deposition reaches the peak (e.g. case 3 shown in Figure 9(c)). Except for case 3, the position x_D', where the simulated sediment deposition reaches the peak value, is always ahead of the adjustment region length x_D derived from the study of Chen et al. (2013). These results indicate that the vertical updraft seems to disappear ahead of the calculated x_D, which was also verified by the results shown in Figure 3(b) in the study of Follett and Nepf (2017). The net deposition, therefore, reaches the maximum value ahead of x_D.

The total deposition in cases 1, 2 and 3 is larger than that in the cases 4, 5 and 6, while the deposition probability of cases 1, 2 and 3 is considerably smaller than that in cases 4, 5 and 6. This phenomenon may be ascribed to two facts. First, for cases 1 and 2, although the sediment deposition probability is small due to small flow velocity and weak turbulence intensity, the resuspension rarely exists under the effect of the weak turbulence, leading to the large total deposition. In these conditions, the effect of the vegetation and the shear stress on the sediment deposition is nearly comparable. Second, on the one hand, with the bulk velocity of case 3 increasing to the same magnitude of cases 4, 5 and 6, the turbulent intensity is no longer small

than that in the other cases. In this situation, the aquatic vegetation plays an important role on the deposition, which is dramatically different from the low current condition. This means that the deposition probability is small because of the strong turbulence. On the other hand, dense vegetation, which means more obstructions, generates small sand-carrying capacity of flow and large net deposition, as verified by cases 3, 4 and 5 (deposition increases with the increase of the vegetation density). According to these two factors, the vegetation density of case 3 is three or five times of other cases, and the flow velocity is large enough to induce intensive turbulence. Therefore, the net deposition of case 3 is large while its deposition probability is small.

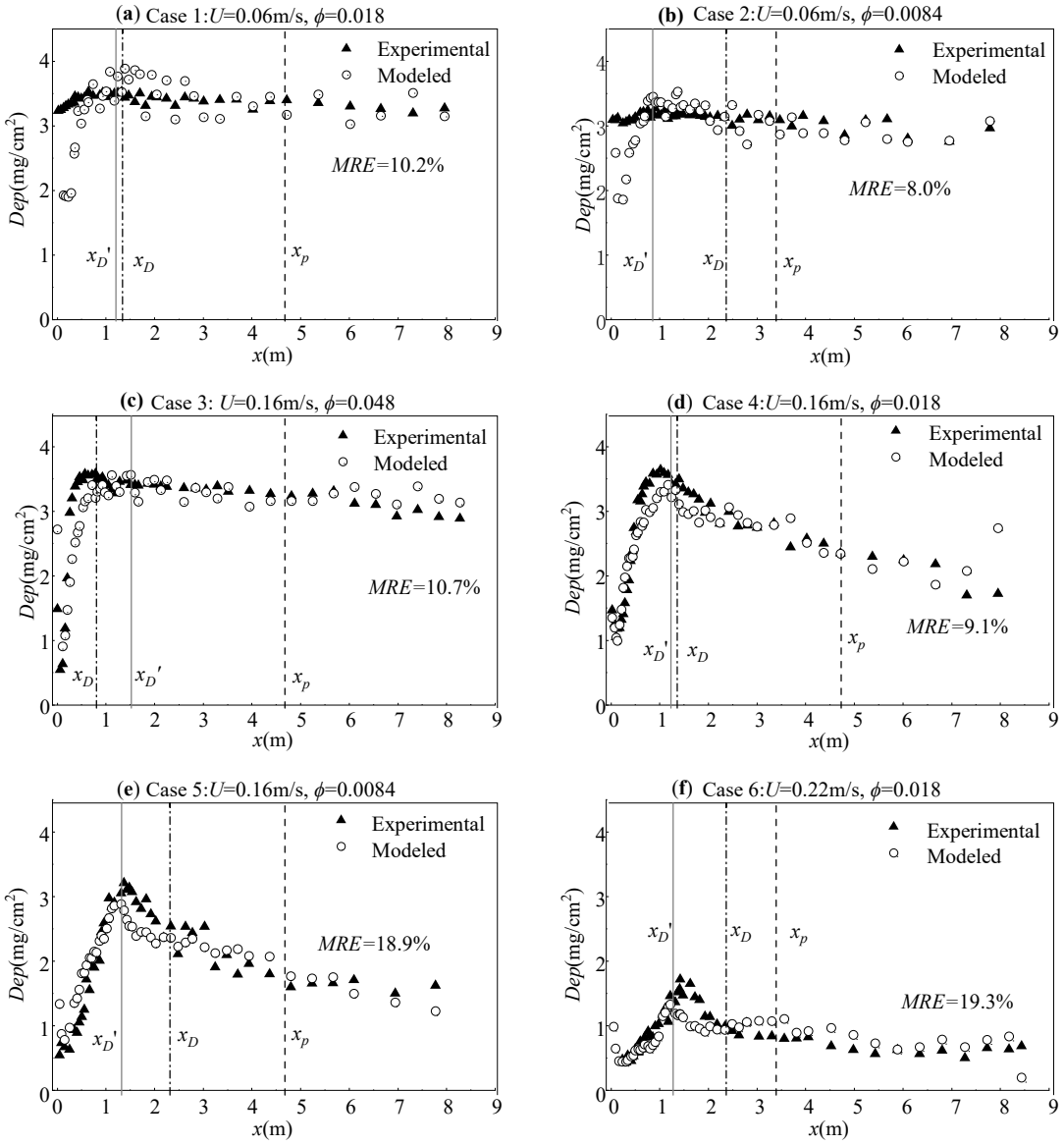

Figure 9 Predicted and experimentally measured sediment deposition profiles. The vertical solid lines show the position of maximum sediment deposition (x_D') in the model; while the dot dash lines and dash lines are the end of the adjustment (x_D) and transition regions (x_p), respectively, and the two lines divide the vegetation patch into three parts.

3.3 Relevance of the Turbulent Kinetic Energy to Sediment Motions

The turbulent kinetic energy is used as a characteristic parameter of the turbulence to explore the relationship between the net sediment deposition/resuspension and the turbulent intensity. As discussed above, the sediment incipient motion is closely related to the turbulent kinetic energy. This is because the turbulence dominates the sediment transport in the vegetation region in the vegetated sediment laden flow; while in the bare-bed channel flow, it is the shear stress that determines the sediment transport. According to the study of Tanino and Nepf (2008), the vegetation-induced turbulent kinetic energy, k [L^2T^{-2}], can be expressed as follows:

$$k = \delta^2 \left(\frac{2C_D\phi}{\pi(1-\phi)} \right)^{2/3} U^2 \quad (21)$$

The scale factor δ=1.1 is used in this study when the ratio of the vegetation stem diameter and the mean interval between stems is smaller than 0.56 (Tanino & Nepf, 2008). The sediment motion in the flow is closely related to the sediment intrinsic characteristic, such as sediment size or relative density, and flow characteristics, such as flow velocity or turbulent kinetic energy. In order to analyze the relationship between turbulent kinetic energy and sediment motion, the turbulent kinetic energy can be normalized by the characteristic parameter of the sediment particles, that is, $(s\text{-}1)gd_{50}$, which is similar to the method of the Shields number. The dimensionless turbulent kinetic energy ψ can then be written as follows:

$$\psi = \frac{\delta^2}{(s-1)gd_{50}} \left(\frac{2C_D\phi}{\pi(1-\phi)} \right)^{2/3} U^2 \quad (22)$$

3.3.1 Relevance to Deposition

Figure 10 shows the variation of the deposition probability P_{d1} with the dimensionless turbulent kinetic energy ψ, demonstrating the effect of the turbulence induced by the vegetation on the sediment deposition. Figure 10 shows that the deposition probability decreases with the increase of the turbulent kinetic energy when ψ ranges from 10 to 37 according to the conditions of Cases 3, 4, 5 and 6. This situation can be understood from the effect of the vegetation-induced turbulent kinetic energy on the sediment movement. The sediment deposition is inhibited by the intense turbulence, as found in the study of Kim et al. (2018). This phenomenon can be explained by the underlying mechanisms of the sediment deposition and the resuspension. The close relationship between the sediment movement and the flow field features indicates that the strong turbulent vortex enhances the sediment resuspension and weakens the sediment deposition. Furthermore, the sediment particles usually move upward due to the vortices induced by the vegetation (Tinoco & Coco, 2016). Therefore, both the sediment concentration near the channel bed and the virtual deposition layer decreases. Engelund and Fredsoe (1976) showed that the incipient sediment motion didn't complete at a moment; by contrast, the upper sediment was easily suspended by the flow. From this aspect, the reduction in the upper layer, $\Delta C(t, x, dz/2)$, is larger than that in the virtual deposition layer, $\Delta C(t, x, -dz/2)$, when turbulent intensity is enhanced, that is, ψ increases. As a consequence, the sediment deposition probability is smaller compared with the deposition probability in the condition of the weak turbulent kinetic energy according to Equation (9).

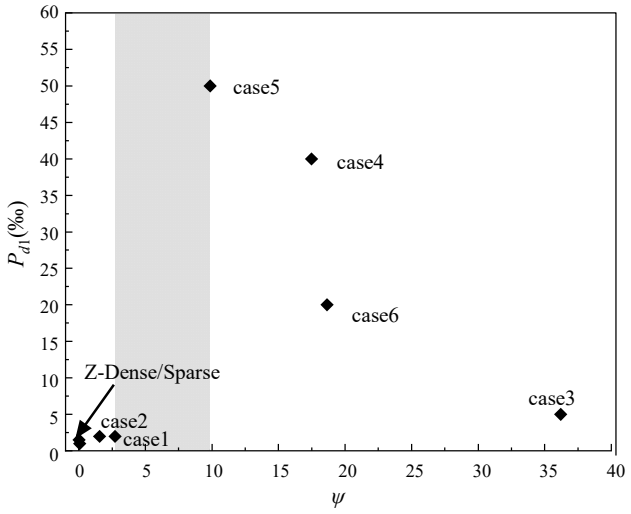

Figure 10 Variation of the sediment deposition probability (represented by the deposition probability outside the adjustment region P_{d1}) with the dimensionless turbulent kinetic energy ψ. The gray block indicates the scope of the critical turbulent kinetic energy.

For conditions "cases 1 and 2, Z-dense and Z-sparse," represented by "Small case" hereafter, the flow velocity and the stem Reynolds number are much smaller than that in Cases 3, 4, 5 and 6 (see Tables 1 and 2). The deposition probability P_{d1}=1 or 2‰ for the "Small cases" is quite similar to that in the channel without vegetation, and the corresponding turbulent kinetic energy is in the range $0<\psi<2.5$. The weak turbulence intensity induced by small velocity and the stem Reynolds number has a weak impact on the sediment deposition and the resuspension comparing with the situation in the bare-bed channel flow. The deposition probability is the same as that in the bare-bed channel, and the net sediment deposition profile is nearly a flat level in the vegetation patch region. In the "Small cases", the increased turbulent kinetic energy cannot enhance the sediment deposition probability, indicating that there exists a critical value of ψ before the impact of the canopy induced turbulent kinetic energy, which dominates the sediment motion. The result shows that the critical value of ψ, represented as ψ_*, is from 2.5 to 10.

Above analysis shows that the flow velocity and the vegetation density are the main factors affecting the turbulent kinetic energy (see also Equation (22)). However, the present study shows that these two factors probably affect the turbulent kinetic energy in different ways. The depth-averaging flow velocity represents the state of the whole current movement and plays a more important role on the turbulent kinetic energy than that played by the vegetation density, as indicated by the different indices of U and ϕ in Equation (22). The results of the present study suggest that if the velocity is small (e.g. similar to the "Small cases"), the effect of the vegetation on the deposition is then minimal no matter it is dense or sparse vegetation. When the flow velocity is sufficiently large to generate the strong turbulence, the vegetation effect starts to become significant. The deposition probability decreases continuously with the increase of the vegetation density as illustrated by cases 3, 4 and 5, as shown in Figure 10.

3.3.2 Relevance to Resuspension

The particles resuspension motion could be promoted by the turbulence. Zhang et al (2020) took the deposition in cases 1 and 2 (3.24 ± 0.16 mg/cm^2) as the inferred deposition without resuspension, and calculated the sediment resuspension according to the deviation

552 between measured net deposition and this inferred deposition. Adapting the same method as
553 Zhang et al (2020), Figure 11 shows the comparison of the simulated and measured resuspension,
554 M_res [ML^{-2}] (Figure 11 (a), and the relationship between the resuspension and dimensionless
555 turbulent kinetic energy, ψ (Figure 11(b)) Good agreement between the simulated and
556 experimentally measured resuspension further verifies the present model. From Figure 11(b), the
557 resuspension is small for ψ<6.8 and then increases with the increase of the turbulent kinetic
558 energy. This implies that there exists a critical turbulent kinetic energy, i.e.ψ_*=6.8 in this study,
559 which is also within the range of the threshold inferred from analysis about deposition and ψ (see
560 Figure 10). Considering the relationship between both the deposition and resuspension with the
561 turbulent kinetic energy, the critical ψ can be further estimated as 6.8<ψ_*<10. This means that
562 when the turbulent kinetic energy is above the threshold, the turbulence induced by vegetation
563 dominates the sediment particles motions, namely the deposition and resuspension.

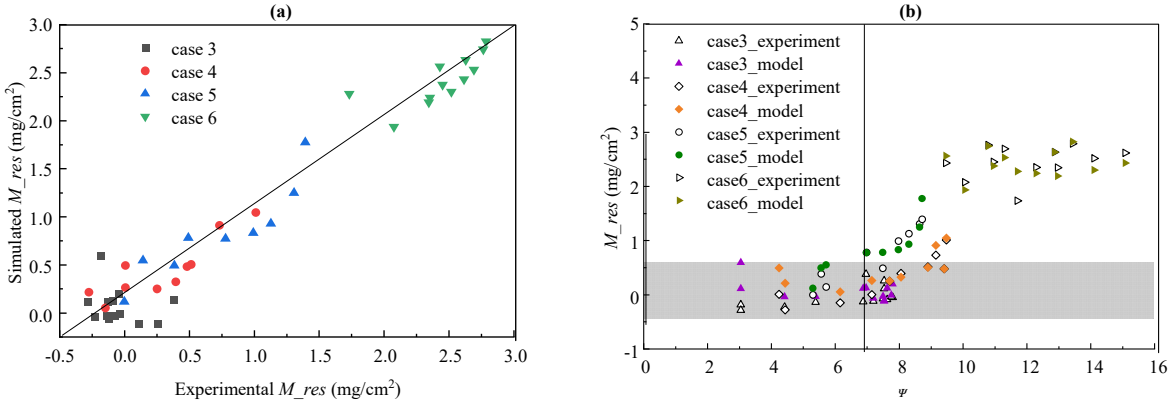

564

565 **Figure 11** (a) Comparison of experimentally measured and simulated resuspension; (b)
566 relationship between the resuspension and the dimensionless turbulent kinetic energy. The gray
567 square expresses the extent where the impact of the turbulent kinetic energy is insignificant.

568

569 ## 4 Discussion

570 A probability model of the sediment deposition and the resuspension is proposed in this
571 study. The net sediment deposition in the flow with the vegetation patch is simulated by
572 integrating the probability model with the random displacement model. The results show that the
573 turbulent kinetic energy has a more remarkable effect on the sediment deposition and the
574 resuspension than the bed shear stress in the vegetated sediment laden flow. The results also
575 indicate that the effect of the aquatic vegetation on the sediment deposition seems to be
576 significant when the turbulent kinetic energy is larger than the threshold. The present study fills
577 the knowledge gap by integrating the sediment deposition probability and the turbulent kinetic
578 energy. Furthermore, this study also extends the application of the random displacement model
579 to the study of the sediment deposition in the channel with vegetation.

580 ### 4.1 Probability-based Boundary Model

581 The deposition boundary used in this study refers to the sorption boundary of the
582 pollutant (Sankarasubramanian & Gill, 1973; Wang & Huai, 2019). The simulated net deposition
583 agrees well with the experimental measurements because the sediment particles in the present

study are small, that is, d_{50}=7 μm in the study of Zhang et al. (2020) and d_{50}=12 μm in the experiments of Zong and Nepf (2010). The approach as to whether settling velocity is considered or not is the main difference between the sediment and the pollutant whose settling velocity is usually ignored. Therefore, the transport of fine sediments may be similar to that of the pollutant because the settling velocity is small. Figures 8 and 9 show that the deviation between the simulated and measured deposition in the experiment of Zong and Nepf (2010) is larger than that in the experiments of Zhang et al. (2020), which could be due to the difference in the sediment diameter in these two experiments. Furthermore, the whole variation tendency of the observed deposition in the experiments of Zong and Nepf (2010) along the streamwise direction in the downstream of the adjustment region is much flatter than the simulated deposition. This result demonstrates that the particles diameter has an effect on the accuracy of this model. Overall, the model proposed in this study is applicable to the fine sediment as the approach of the deposition boundary is a progress in the theory of sorption boundary for pollutant.

To simulate the sediment motion characteristics, i.e. deposition and resuspension, we adapt the pure sorption boundary to probability-based boundary. Taking cases 3, 4 and 5 as examples, Figure 12 shows the comparison of the sediment deposition patterns with the pure sorption boundary and the probability-based boundary, respectively. The pure sorption boundary ignores the fact that the sediment particles, which temporarily reach the riverbed, could not stay there completely and the majority of the sediment particles will be carried by the turbulence departing the river bed. Therefore, the pure sorption boundary poorly models the sediment deposition in the channel with canopy. However, the probability-based boundary model takes this instability of particles motion into account with the probability model adapting to the flow field structure. In addition, there is large modeled deposition deviation between the probability-based and the sorption boundary in the leading of vegetation, indicating that the impact of updraft in the adjustment region plays an important role in the sediment motion. The comparison reveals the superiority of the present model in simulating the sediment deposition in channels with vegetation.

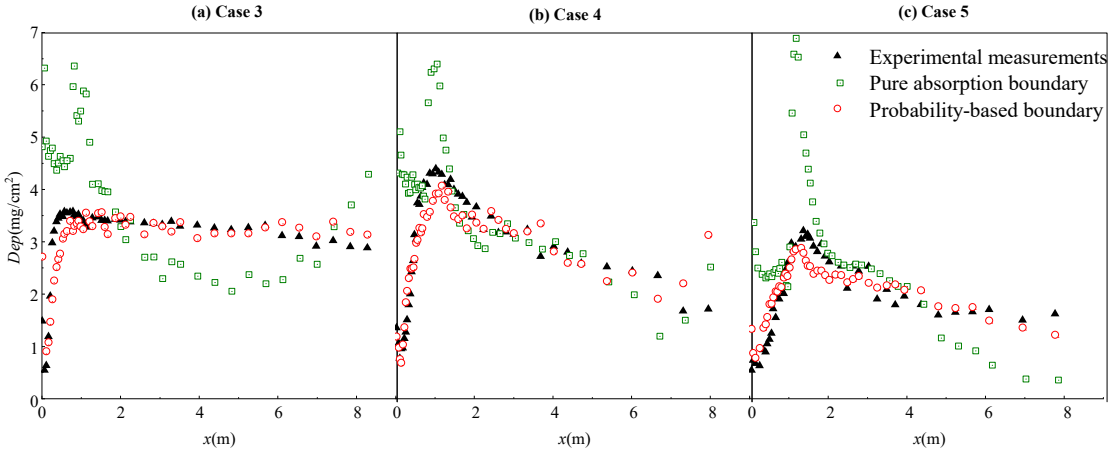

Figure 12 Comparison of the experimentally measured deposition (black solid triangles) and the simulated deposition patterns with the pure sorption boundary (green open squares) and the probability-based boundary (red open circles).

The probability model proposed in this study can reveal the interaction between the vegetation and the sediment deposition and resuspension. The resuspension probability is derived from the probability density function of the near-bed averaging flow velocity, while the deposition probability must be calibrated by experimental data. To better describe the deposition probability, sufficient experimental data are required. Although the experimental data are limited, this study illustrates several findings through analyzing the dimensionless turbulent kinetic energy and investigating the relationship between the sediment deposition probability and the turbulent kinetic energy. The analysis shows that within the scope of ψ investigated in this study, the deposition probability decreases with the increase of the turbulent kinetic energy when the turbulence kinetic energy is larger than its threshold. The effect of the vegetation on the sediment deposition prevails when the turbulent kinetic energy is larger than the critical value. However, the problem has not been quantitatively analyzed; and the formula used to determine the deposition probability, which is acknowledged difficult to overcome, is not derived due to the limited experimental data. Further experiments are also required to explore the relationship between sediment motions and the turbulent kinetic energy.

4.2 Particles motions

Note that the calculated resuspension conducted in Zhang et al (2020) is a relative value, which means that all calculated resuspension is relative to the averaged deposition in the cases 1 and 2. They explained that the resuspension motion accounted for the lower deposition in other cases. The method could, to some extent, show the effect of flow field characteristics on the deposition and resuspension within a long experiment period (e.g. 4 hours in the experiment) through analyzing the relative value in different condition. However, it is difficult for the method to clarify the process of sediment particles deposition and resuspension motions. In present study, the numerical model, i.e. the random displacement model, tracks particles motion; the deposition and resuspension could be clarified through accounting the number of deposition and resuspension particles, respectively.

Taking case 3 as an example, Figure 13 shows the total deposition without resuspension, measured and modeled deposition with resuspension, and the simulated resuspension in the process of simulation. The validity of the model has been discussed above, therefore, we expect to infer sediment particles motion from the model. According to present model, the deposition probability in the leading of head is small with the effect of updraft, while the resuspension probability, calculated from the near-bed velocity, is a constant in the whole domain. From Figure 13, the pattern of resuspension along the longitudinal direction is the same as the deposition without resuspension, although the pattern of deposition and resuspension probability is different from each other in the adjustment region. It is also found that the magnitude of deposition is larger than resuspension. The result indicates the effect of the deposition motion on the pattern of final deposition is relatively more important than resuspension motion. The experiments of the sediment deposition discussed in this study were conducted by feeding sediment in the upstream of the flume. This means that particles deposition in the bed is the precondition of the resuspension. Therefore, the finding is consistent with the concept of resuspension. For another experiment method, i.e. paving sediment layer in the river bed (Tinoco & Coco, 2016), it is obvious that resuspension dominates the sediment particles motion, and the deposition was ignored in the study. The different experimental methods may interpret two completely different findings between present study and Tinoco and Coco (2016). From the results of the present model, it is important for the resuspension analysis to clarify its definition.

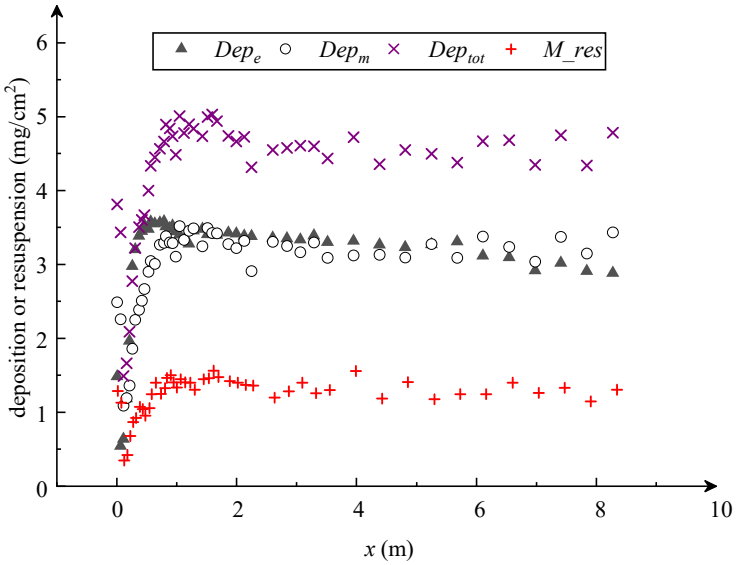

Figure 13 Deposition measured in the experiment case 3, Dep_e (gray triangles); simulated deposition Dep_m (circles) with resuspension; total deposition Dep_{tot} (purple forks) without resuspension; and the simulated resuspension M_res (red crosses).

The random displacement model has been successfully applied to simulate the vertical profile of the suspended sediment concentration in the full developed state (Huai et al., 2019). The boundary condition at the channel bottom proposed in this study associates the deposition and resuspension probability model and further expands the application of the random displacement model in the study of sediment deposition within the aquatic vegetation region. The proposed model is an innovative methodology for simulating the sediment deposition in the vegetated sediment laden channel flow, which may considerably promote the development of the sediment deposition studies.

5 Conclusions

This study simulates the profile of the net sediment deposition in the vegetation patch and focuses on investigating the effect of the turbulent kinetic energy on the deposition probability through an innovative random displacement model. The deposition probability increases from zero at the leading edge of the vegetation patch ($x<x_D$) and maintains a constant value at the region $x>x_D$. The resuspension probability is derived from the probability density function of the flow velocity near the channel bed by assuming that the sediment resuspension occurs when the instantaneous velocity is larger than the critical velocity of the incipient sediment motion. The following conclusions can be drawn from this study:

(1) The sediment deposition probability is closely related to the turbulent kinetic energy ψ. The effect of the turbulent kinetic energy induced by the aquatic vegetation on the sediment deposition is similar to the effect of the shear stress in the bare-bed channel when ψ is small. By contrast, the turbulent kinetic energy dominates the sediment deposition when the value of ψ is larger than the critical value ψ_*, and the deposition probability decreases with the increase of ψ for $\psi> \psi_*$.

(2) The threshold of the turbulent kinetic energy ψ_* is an important parameter in the deposition studies because the effect of the vegetation on the sediment deposition and resuspension begins to prevail when $\psi > \psi_*$. In the present study, the threshold cannot be derived directly due to the limited experimental data; however, the range of 6.8 to 10 is recommended as the critical value based on the analysis of the simulation. Further experiments are needed to determine the specific threshold of the turbulent kinetic energy.

(3) The innovative random displacement model proposed in this study extends the application of the model on the sediment deposition with the improvement of the probability-based deposition and resuspension boundary rather than the pure sorption boundary. The model is validated by the good agreement between the simulated and measured net sediment deposition. From the comparison of the probability-based boundary and pure the sorption boundary, the present model is much accurate for simulating the real particle motion near the channel bed, which suggests an improvement in the random displacement model.

(4) In the present model, the deposition probability is used to illustrate the sediment motion at the leading edge of the vegetation patch, while both the resuspension and the deposition are rationally considered beyond the adjustment region. This study demonstrates that the main effect of the vegetation on the sediment transport varies at the different regions of the vegetation patch, which helps to investigate the underlying physical mechanism of the sediment transport near the channel bed.

Acknowledgments

All the data used in this work have been reported elsewhere (Zhang et al., 2020; Zong & Nepf, 2010). The research reported here is financially supported by the Natural Science Foundation of China (Nos. 52020105006 and 11872285), The UK Royal Society – International Exchanges Program (IES\R2\181122) and the Open Funding of State Key Laboratory of Water Resources and Hydropower Engineering Science (WRHES), Wuhan University (Project No: 2018HLG01).

There are no real or perceived financial conflicts of interests for any author, no other affiliations for any author that may be perceived as having a conflict of interest with respect to the results of this paper.

720 **Appendix** Data bank collected from previous experiment Zong and Nepf (2010) and Zhang et al
721 (2020) and the corresponding simulated net sediment deposition with RDM in present model.

Z_dense			Z_sparse		
x(m)	Dep_e(mg/cm^2)	Dep_m(mg/cm^2)	x(m)	Dep_e(mg/cm^2)	Dep_m(mg/cm^2)
0.3081			0.1152	1.3309	0.3335
0.6168			0.2001	1.4766	0.5704
1.2263			0.3283	2.1280	0.8993
1.8357			0.4065	1.7648	1.0327
2.4451			0.5197	1.6493	1.4996
3.0686			0.6328	2.3143	1.6560
3.6599			0.9341	2.9938	2.5024
4.2874			1.2619	2.6753	2.5024
4.8908			1.5698	3.3236	2.9992
5.5022			1.8744	3.2778	3.2154
6.1076			2.1107	3.4568	3.5006
6.7231	2.0097	0.9906	2.4735	3.3881	3.7536
7.3325	2.6719	1.9290	2.7648	3.5307	3.9238
7.9359	3.0286	3.1314	3.0644	3.4422	3.8709
	3.1568	3.6468	3.3140	3.5931	3.9353
	3.2717	3.5328	3.7234	3.4537	3.6064
	3.3450	3.3510	4.0130	3.6556	3.7030
	3.0212	3.2094	4.3176	3.5765	3.5581
	3.0066	3.0186	4.5672	3.6504	3.4615
	3.1202	2.8122	4.9134	3.5307	3.3120
	3.0762	2.6850	5.5175	3.4433	3.1901
	2.6303	2.2758	6.1250	3.2383	3.0774
	2.7232	2.2164	6.7291	3.1415	2.7968
	2.4104	1.9302	7.4298	3.2466	2.5162
	2.2333	1.9404			

Case 1			Case 2		
x(m)	Dep_e(mg/cm^2)	Dep_m(mg/cm^2)	x(m)	Dep_e(mg/cm^2)	Dep_m(mg/cm^2)
0.1307	3.2792	1.9247	0.0912	3.0894	2.5845
0.1767	3.3060	1.9126	0.1368	3.1242	1.8763
0.2281	3.3329	1.9005	0.2439	3.0403	1.8582
0.2883	3.3474	1.9611	0.3124	3.0618	2.1729
0.3504	3.3629	2.5663	0.3721	3.0966	2.5845
0.3610	3.4579	2.6632	0.4546	3.0873	2.7237
0.4265	3.4403	3.2321	0.5002	3.1344	2.7782
0.4886	3.4217	3.0384	0.5985	3.2050	3.0384
0.5559	3.4372	3.2563	0.6617	3.2142	3.0687
0.6214	3.4548	3.4016	0.6915	3.1170	3.1474
0.6374	3.5292	3.3653	0.7565	3.2419	3.3834
0.7348	3.4672	3.6437	0.8127	3.1303	3.4318
0.8730	3.4785	3.2684	0.8636	3.1897	3.4500

0.9333	3.5147	3.4621	0.9110	3.2716	3.3592
1.0059	3.4455	3.5347	0.9707	3.1692	3.3653
1.0821	3.5023	3.8374	1.0216	3.1692	3.3653
1.1689	3.5023	3.3895	1.1199	3.2542	3.1413
1.2415	3.5147	3.7647	1.1743	3.1078	3.3290
1.3284	3.5292	3.5226	1.2603	3.1518	3.2745
1.3886	3.4372	3.8858	1.3323	3.1518	3.4863
1.4701	3.4723	3.7163	1.3709	3.1968	3.5287
1.5941	3.3711	3.8616	1.4306	3.2245	3.2926
1.7004	3.5054	3.8011	1.4867	3.1774	3.3229
1.8138	3.3143	3.1474	1.6237	3.1672	3.2563
1.9414	3.4517	3.7890	1.7255	3.1774	3.3471
2.0442	3.4403	3.4863	1.8325	3.1600	3.2382
2.2444	3.4248	3.7042	1.9361	3.1426	3.3168
2.4233	3.3112	3.0990	2.0291	3.1324	3.0747
2.6217	3.4403	3.6921	2.1924	3.1569	2.9355
2.8113	3.4217	3.4621	2.3363	3.1303	3.1413
3.0062	3.3804	3.1353	2.4908	3.0024	3.3229
3.3429	3.4042	3.1111	2.6418	3.0996	2.9234
3.6813	3.4073	3.4500	2.7945	3.1774	2.7116
4.0232	3.2523	3.3047	3.0262	3.0925	3.1716
4.3722	3.3835	3.4500	3.2614	3.1518	3.0747
4.7142	3.3980	3.1716	3.4738	3.0925	2.8690
5.3644	3.3536	3.4863	3.7143	2.9932	3.1353
6.0182	3.3029	3.0263	3.9478	3.1569	2.8871
6.6525	3.2616	3.1595	4.3673	3.0771	2.8871
7.3081	3.1986	3.5105	4.8026	2.8561	2.7782
7.9583	3.2730	3.1474	5.2327	3.0894	3.0566
			5.6733	3.1027	2.7963
			6.0999	2.8039	2.7540
			6.9512	2.7588	2.7721
			7.7833	2.9635	3.0747

	Case 3			Case 4	
x(m)	Dep_e(mg/cm^2)	Dep_m(mg/cm^2)	x(m)	Dep_e(mg/cm^2)	Dep_m(mg/cm^2)
0.1118	0.6368	0.9079	0.0194	1.4680	1.3497
0.1639	1.1887	1.0774	0.0739	1.2562	1.1984
0.0057	1.4861	2.7176	0.1051	1.0531	1.0411
0.2102	1.9642	1.4708	0.1324	1.1830	0.9926
0.2604	2.9799	1.9005	0.1792	1.1918	1.2408
0.3048	3.2035	2.2576	0.2162	1.3217	1.4768
0.3685	3.3863	2.5179	0.2532	1.4101	1.8158
0.4186	3.4502	2.6692	0.2883	1.5782	1.9732
0.4611	3.5307	2.7721	0.3331	1.7835	2.1487
0.5286	3.4800	3.0626	0.3682	1.9320	2.2758

0.5672	3.5758	3.1534	0.4033	2.2311	2.2758
0.7177	3.5648	3.4016	0.4461	2.3872	2.2940
0.6347	3.5527	3.2018	0.4715	2.7409	2.4090
0.7871	3.5802	3.2079	0.5163	2.6776	2.6268
0.8219	3.5119	3.3047	0.5514	3.1732	2.6692
0.8817	3.4866	3.3532	0.6040	3.1547	2.8326
0.9280	3.5229	3.4016	0.6391	3.2649	2.7721
0.9820	3.4447	3.2926	0.6722	3.3861	2.8266
1.0476	3.4040	3.2442	0.7131	3.4483	3.0203
1.1229	3.3390	3.5590	0.7930	3.4276	2.9840
1.2078	3.2806	3.3895	0.8651	3.5804	3.0505
1.2811	3.4579	3.2987	0.9392	3.5684	3.2018
1.4277	3.4778	3.5468	1.0191	3.6416	3.2987
1.5145	3.4095	3.5650	1.0892	3.5935	3.3047
1.5936	3.4073	3.2866	1.1711	3.5630	3.4076
1.6689	3.3974	3.1474	1.2412	3.4221	3.2140
1.8618	3.4271	3.4500	1.3289	3.4232	3.3290
1.9950	3.4139	3.4863	1.3932	3.4953	3.1111
2.1281	3.3863	3.3290	1.4809	3.3566	2.9900
2.2477	3.3808	3.4742	1.5900	3.2922	2.9537
2.6027	3.3599	3.1413	1.6992	3.2617	3.0021
2.8381	3.3533	3.3592	1.8083	3.1798	2.8266
3.0600	3.3346	3.2926	1.9369	2.9811	3.0142
3.2877	3.3919	3.1958	2.0460	3.1208	2.9053
3.5154	3.3004	3.3774	2.2370	2.8086	2.8205
3.9514	3.3191	3.0687	2.4241	2.9942	3.0626
4.3836	3.2674	3.1595	2.6131	2.7682	2.9416
4.8139	3.2332	3.1595	2.8041	2.7791	2.8205
5.2518	3.2729	3.1595	3.0009	2.7486	2.7600
5.6802	3.3114	3.2745	3.3478	2.8141	2.7842
6.1085	3.1176	3.3774	3.6868	2.4451	2.8932
6.5446	3.0977	3.2684	4.0220	2.5793	2.5118
6.9787	2.9193	3.1050	4.3728	2.5029	2.3545
7.4089	3.0206	3.3834	4.7157	2.3523	2.3424
7.8431	2.9094	3.1897	5.3705	2.2999	2.1063
8.2772	2.8862	3.1353	6.0155	2.2464	2.2213
			6.6664	2.1831	1.8642
			7.3114	1.6972	2.0761
			7.9506	1.7245	2.7358

	Case 5			Case 6	
x(m)	Dep_e(mg/cm^2)	Dep_m(mg/cm^2)	x(m)	Dep_e(mg/cm^2)	Dep_m(mg/cm^2)
0.0482	0.5454	1.3356	0.2347	0.4764	0.4418
0.0887	0.7361	0.8756	0.3086	0.4399	0.4439
0.1494	0.6726	0.7808	0.3455	0.5387	0.4701

0.2561	0.6302	0.9684	0.4156	0.4582	0.5246
0.3499	0.9354	1.3538	0.4580	0.5323	0.5427
0.4088	0.8941	1.4244	0.5005	0.6408	0.6194
0.4493	1.0509	1.5596	0.5595	0.5914	0.6375
0.5063	1.1378	1.8118	0.6019	0.7557	0.6275
0.5541	1.2491	1.8198	0.6610	0.6805	0.6618
0.6019	1.7196	1.9368	0.6923	0.8201	0.7082
0.6627	1.5532	2.0539	0.7606	0.9104	0.6840
0.7013	1.9231	2.0478	0.7975	0.8610	0.6456
0.7583	1.9040	2.1507	0.8566	0.8234	0.7021
0.8061	2.0821	2.1325	0.9101	0.9963	0.7465
0.8705	2.0100	2.3141	0.9784	1.0274	0.8373
0.9092	2.4541	2.3928	1.0595	1.1735	1.1480
0.9588	2.5887	2.3444	1.1758	1.0618	1.2953
1.0195	2.6417	2.5058	1.1167	1.2659	1.2045
1.0618	2.9755	2.6632	1.2182	1.4646	1.3296
1.1189	2.8441	2.8165	1.3197	1.3647	1.1883
1.1704	2.9066	2.8568	1.3677	1.5204	1.1621
1.3139	3.0507	2.8831	1.4101	1.5698	1.1843
1.3709	3.2118	2.7883	1.4212	1.7181	1.1783
1.4261	3.1037	2.6410	1.4784	1.4732	1.1278
1.4776	3.1408	2.5441	1.6279	1.6504	0.9886
1.5383	3.0719	2.5340	1.7238	1.4420	1.0007
1.6229	2.9172	2.3888	1.8198	1.3991	0.9583
1.7223	2.8112	2.4513	1.9305	1.1424	0.9099
1.8234	2.9607	2.4473	2.0319	1.1391	0.9906
1.9228	2.7275	2.3646	2.1814	1.0242	0.9422
2.0276	2.6162	2.2738	2.3401	0.9877	0.9382
2.1840	2.3651	2.3726	2.4896	0.9222	1.0269
2.3312	2.5378	2.3625	2.6279	0.8545	0.9765
2.4839	2.1107	2.2254	2.7922	1.0489	1.0592
2.6329	2.5357	2.2879	3.0431	0.8330	1.0754
2.7800	2.4382	2.3464	3.3033	0.8384	1.0733
3.0247	2.5325	2.2173	3.5579	0.8019	1.1036
3.2455	1.9051	2.1225	3.8089	0.8083	0.8918
3.4864	2.0937	2.1668	4.0580	0.8266	0.9160
3.7054	1.7959	2.1870	4.5248	0.6869	0.9644
3.9390	1.9623	2.0801	4.9768	0.6279	0.8575
4.3603	1.7991	2.0700	5.4289	0.5667	0.7304
4.7999	1.5999	1.7674	5.8865	0.6257	0.6335
5.2341	1.6539	1.7311	6.3386	0.5634	0.6698
5.6701	1.6603	1.7512	6.8036	0.6182	0.7889
6.0950	1.7069	1.4950	7.2704	0.5011	0.6698
6.9449	1.5034	1.3618	7.7280	0.6590	0.7828
7.7709	1.6232	1.2247	8.1801	0.6375	0.8353

	8.4347	0.6837	0.1957

References

Abt, S., Clary, W. P., & Thornton, C. (1994). Sediment Deposition and Entrapment in Vegetated Streambeds. *Journal of Irrigation and Drainage Engineering*, 120(6), 1098-1111. https://doi.org/10.1061/(ASCE)0733-9437(1994)120:6(1098)

Ai, Y. D., Liu, M., Huai, W. X. (2020). Numerical investigation of flow with floating vegetation island. Journal of Hydrodynamics, 32(1):31-43. https://doi.org/10.1007/s42241-020-0004-6

Beheshti, A. A., & Ataie-Ashtiani, B. (2008). Analysis of threshold and incipient conditions for sediment movement. *Coastal Engineering*, 55(5), 423-430. https://doi.org/10.1016/j.coastaleng.2008.01.003

Beuselinck, L., Steegen, A., Govers, G., Nachtergaele, J., Takken, I., & Poesen, J. (2000). Characteristics of sediment deposits formed by intense rainfall events in small catchments in the Belgian Loam Belt. *Geomorphology*, 32(1), 69-82. https://doi.org/10.1016/S0169-555X(99)00068-9

Chen, Z., Jiang, C., & Nepf, H. M. (2013). Flow adjustment at the leading edge of a submerged aquatic canopy. *Water Resources Research*, 49(9), 5537-5551. https://doi.org/10.1002/wrcr.20403

Cheng, N. S. (1997). A simplified settling velocity formula for sediment particle. *Journal of Hydraulic Engineering*, 123(2),149-152. https://doi.org/ 10.1061/(ASCE)0733-9429(1997)123:2(149)

Choi, S., & Kwak, S. (2001). Theoretical and Probabilistic Analyses of Incipient Motion of Sediment Particles. *KSCE Journal of Civil Engineering*, 5(1), 59-65. https://doi.org/10.1007/BF02830727

Diplas, P., Dancey, C. L., Celik, A. O., Valyrakis, M., Greer, K., & Tanju, A. (2008). The Role of Impulse on the Initiation of Particle Movement Under Turbulent Flow Conditions. *Science*, 322(5902), 717-720. https://doi.org/10.1126/science.1158954

Dou, G. R. (1960). On Velocity of Incipient Motion. *Journal of Hydraulic Engineering*, 2(4), 46-62 (in Chinese). https://doi.org/CNKI:SUN:SLXB.0.1960-04-003

Engelund, F., & Fredsoe, J. (1976). A Sediment Transport Model for Straight Alluvial Channels. *Nordic Hydrology*, 7(5), 293-306. https://doi.org/10.2166/nh.1976.0019

Follett, E., & Nepf, H. M. (2012). Sediment patterns near a model patch of reedy emergent vegetation. *Geomorphology*, 179, 141-151. https://doi.org/10.1016/j.geomorph.2012.08.006

Follett, E., Chamecki, M., & Nepf, H. M. (2016). Evaluation of a random displacement model for predicting particle escape from canopies using a simple eddy diffusivity model.

Agricultural and Forest Meteorology, 224, 40-48. https://doi.org/10.1016/j.agrformet.2016.04.004

Follett, E., & Nepf, H. M. (2018). Particle Retention in a Submerged Meadow and Its Variation Near the Leading Edge. *Estuaries and Coasts*, 41(3), 724-733. https://doi.org/10.1007/s12237-017-0305-3

Follett, E., Hays, CG, & Nepf, H. M. (2019). Canopy-Mediated Hydrodynamics Contributes to Greater Allelic Richness in Seeds Produced Higher in Meadows of the Coastal Eelgrass Zostera marina. Frontiers in Marine Science, 6:8. https://doi.org/10.3389/fmars.2019.00008

Gacia, E., Duarte, C. M., Marbà, N., Terrados, J., Kennedy, H., & Fortes, M. D., et al. (2003). Sediment deposition and production in SE-Asia seagrass meadows. *Estuarine, Coastal and Shelf Science*, 56(5-6), 909-919. https://doi.org/10.1016/S0272-7714(02)00286-X

Ghisalberti, M. (2002). Mixing layers and coherent structures in vegetated aquatic flows. *Journal of Geophysical Research*, 107(C2). https://doi.org/10.1029/2001JC000871

Ghisalberti, M., & Nepf, H. M. (2004). The limited growth of vegetated shear layers. *Water Resources Research*, 40(7). https://doi.org/10.1029/2003WR002776

Ghisalberti, M., & Nepf, H. M. (2005). Mass Transport in Vegetated Shear Flows. *Environmental Fluid Mechanics*, 5: 527-551. https://doi.org/10.1007/s10652-005-0419-1

Guo, Y. (2020). Empirical Model for Shields Diagram and Its Applications. *Journal of Hydraulic Engineering*, 146(6), 4020038. https://doi.org/10.1061/(ASCE)HY.1943-7900.0001739

Houssais, M., Ortiz, C. P., Durian, D. J., & Jerolmack, D. J. (2015). Onset of sediment transport is a continuous transition driven by fluid shear and granular creep. *Nature Communications*, 6(1). https://doi.org/10.1038/ncomms7527

Huai, W. X., Cheng, Z., & Han, J. (2009). Mathematical model for the flow with submerged and emerged rigid vegetation. *Journal of Hydrodynamics*, 21(5), 722-729. https://doi.org/10.1016/S1001-6058(08)60205-X.

Huai, W. X., Yang, L., Wang, W., Guo, Y. K., Wang, T., & Cheng, Y. (2019). Predicting the vertical low suspended sediment concentration in vegetated flow using a random displacement model. *Journal of Hydrology*, 578, 124101. https://doi.org/10.1016/j.jhydrol.2019.124101

Huai, W. X., Yang, L., & Guo, Y. K. (2020). Analytical Solution of Suspended Sediment Concentration Profile: Relevance of Dispersive Flow Term in Vegetated Channels. *Water Resources Research*, 56(7). https://doi.org/10.1029/2019WR027012

Kim, H. S., Kimura, I., & Park, M. (2018). Numerical Simulation of Flow and Suspended Sediment Deposition Within and Around a Circular Patch of Vegetation on a Rigid Bed. *Water Resources Research*, 54(10), 7231-7251. https://doi.org/10.1029/2017WR021087

Kim, H. S., Kimura, I., & Shimizu, Y. (2015). Bed morphological changes around a finite patch of vegetation. *Earth Surface Processes and Landforms*, 40(3), 375-388. https://doi.org/10.1002/esp.3639

Lawson, S. E., McGlathery, K. J., & Wiberg, P. L. (2012). Enhancement of sediment suspension and nutrient flux by benthic macrophytes at low biomass. *Marine Ecology Progress Series*, 448, 259-270. https://doi.org/10.3354/meps09579

Liu, X. Y., Huai, W. X., Wang, Y., Yang, Z. H., & Zhang, J. (2018). Evaluation of a random displacement model for predicting longitudinal dispersion in flow through suspended canopies. *Ecological Engineering*, 116, 133-142. https://doi.org/10.1016/j.ecoleng.2018.03.004

Marion, A., & Tregnaghi, M. (2013). A New Theoretical Framework to Model Incipient Motion of Sediment Grains and Implications for the Use of Modern Experimental Techniques. In Experimental and Computational Solutions of Hydraulic Problems. Berlin Heidelberg: Springer. https://doi.org/10.1007/978-3-642-30209-1_5

Mark S. Fonseca, Joseph C. Zieman, Gordon W. Thayer, & John S. Fisher. (1983). The role of current velocity in structuring eelgrass meadows. *Estuarine, Coastal and Shelf Science*, 17, 367-380. https://doi.org/10.1016/0272-7714(83)90123-3

Nelson, J. M., Shreve, R. L., McLean, S. R., & Drake, T. G. (1995). Role of near-bed turbulence structure in bed load transport. *Water Resources Research*, 31(8), 2071-2086. https://doi.org/10.1029/95WR00976

Nepf, H. M., Ghisalberti, M., & Murphy, E. & (2007). Retention time and dispersion associated with submerged aquatic canopies. Water Resources Research, 43(4), 436-451. https://doi.org/10.1029/2006WR005362

Nepf, H. M. (2012). Flow and transport in regions with aquatic vegetation. Annual Review of Fluid Mechanics. 44(1), 123-142. https://doi.org/10.1146/annurev-fluid-120710-101048

Nezu, I., & Nakagawa, H. (1993). Turbulence in Open channel flows. Rotterdam, The Netherlands: IAHR Monograph.

Raupach, M. R., Finnigan, J. J., & Brunei, Y. (1996). Coherent eddies and turbulence in vegetation canopies: The mixing-layer analogy. *Boundary-layer meteorology*, 78(3-4), 351-382. https://doi.org/10.1007/bf00120941

Recking, A. (2009). Theoretical development on the effects of changing flow hydraulics on incipient bed load motion. *Water Resources Research*, 45(4). https://doi.org/10.1029/2008WR006826

Stapleton, K., & Huntley, D. A. (1995). Seabed stress determinations using the inertial dissipation method and the turbulent kinetic energy method. *Earth Surface Processes & Landforms*, 20(9), 807-815. https://doi.org/10.1002/esp.3290200906

Tang, C., Lei, J., & Nepf, H. M. (2019). Impact of Vegetation-Generated Turbulence on the Critical, Near-Bed, Wave-Velocity for Sediment Resuspension. *Water Resources Research*, 55(7), 5904-5917. https://doi.org/10.1029/2018WR024335

Tanino, Y., & Nepf, H. M. (2008). Lateral dispersion in random cylinder arrays at high Reynolds number. *Journal of Fluid Mechanics*, 600, 339-371. https://doi.org/10.1017/S0022112008000505

838 Tinoco, R. O., & Coco, G. (2016). A laboratory study on sediment resuspension within arrays of
839 rigid cylinders. *Advances in Water Resources*, 92, 1-9.
840 https://doi.org/10.1016/j.advwatres.2016.04.003

841 Tinoco, R. O., & Coco, G. (2018). Turbulence as the Main Driver of Resuspension in Oscillatory
842 Flow Through Vegetation. *Journal of Geophysical Research: Earth Surface*, 123(5), 891-
843 904. https://doi.org/10.1002/2017JF004504

844 Tsujimoto, T. (1999). Fluvial processes in streams with vegetation. *Journal of Hydraulic*
845 *Research*, 37(6), 789-803. https://doi.org/10.1080/00221689909498512

846 Yager, E. M., & Schmeeckle, M. W. (2013). The influence of vegetation on turbulence and bed
847 load transport. *Journal of Geophysical Research: Earth Surface*, 118(3), 1585-1601.
848 https://doi.org/10.1002/jgrf.20085

849 Yang, J. Q., Chung, H., & Nepf, H. M. (2016). The onset of sediment transport in vegetated
850 channels predicted by turbulent kinetic energy. *Geophysical Research Letters*, 43(21), 11,
851 211-261, 268. https://doi.org/10.1002/2016GL071092

852 Yang, J. Q., & Nepf, H. M. (2018). A Turbulence-Based Bed-Load Transport Model for Bare
853 and Vegetated Channels. *Geophysical Research Letters*, 45(19), 10, 410-428, 436.
854 https://doi.org/10.1029/2018GL079319

855 Yang, J. Q., & Nepf, H. M. (2019). Impact of Vegetation on Bed Load Transport Rate and
856 Bedform Characteristics. *Water Resources Research*, 55(7), 6109-6124.
857 https://doi.org/10.1029/2018WR024404

858 Zhang, J., Lei, J., Huai, W., & Nepf, H. M. (2020). Turbulence and Particle Deposition Under
859 Steady Flow Along a Submerged Seagrass Meadow. *Journal of Geophysical Research:*
860 *Oceans*, 125(5). https://doi.org/10.1029/2019JC015985

861 Zong, L., & Nepf, H. M. (2010). Flow and deposition in and around a finite patch of vegetation.
862 *Geomorphology*, 116(3-4), 363-372. https://doi.org/10.1016/j.geomorph.2009.11.020